
RAT+: Train Dense, Infer Sparse - Recurrence Augmented Attention for Dilated Inference

Xiuying Wei¹ Caglar Gulcehre¹

Abstract

Structured dilated attention has an appealing inference-time efficiency knob: it reduces the FLOPs of the attention and the KV cache size by a factor of the dilation size D , while preserving long-range connectivity. However, we find a persistent failure mode of them -sparsifying a pretrained attention model to a dilated pattern leads to severe accuracy degradation. We introduce **RAT+**, a dense-pretraining architecture that augments attention with *full-sequence recurrence* and *active recurrence learning*. A single RAT+ model is pretrained densely once, then flexibly switched at inference time to dilated attention (optionally with local windows) or hybrid layer/head compositions, requiring only a short 1B-token resolution adaptation rather than retraining separate sparse models. At 1.5B parameters trained on 100B tokens, RAT+ closely matches dense accuracy at $D = 16$ and drops by about 2-3 points at $D = 64$ on commonsense reasoning and LongBench tasks, respectively. Moreover, RAT+ outperforms attention when sparsifying to the top-k block attention. We further scale to 2.6B parameters and 200B tokens and observe the same trend. Code is available at <https://github.com/wimh966/rat-plus>.

1. Introduction

Efficiency has become increasingly important for modern language models, as standard attention (Vaswani, 2017) incurs a quadratic cost in both FLOPs and memory with respect to sequence length. Among many orthogonal approaches to efficiency (e.g. low-bit representations (Jacob et al., 2018) or faster optimization (Jordan, 2023)), a major line of work seeks to sparsify or replace the attention mechanism itself from the architectural perspective. Most of them

¹CLAIRE lab at EPFL, Lausanne, Switzerland. Correspondence to: Xiuying Wei <xiuying.wei@epfl.ch>, Caglar Gulcehre <caglar.gulcehre@epfl.ch>.

can be grouped into two categories: training-from-scratch sparse architecture versus inference-time sparsification.

The first design approach focuses on efficient architectures and trains them from scratch, including structured sparse attention (e.g., delicately designed dilated patterns (Ding et al., 2023; Beltagy et al., 2020), local window attention (Liu et al., 2021; Cohere et al., 2025)), state space (Gu & Dao, 2023; Dao & Gu, 2024), linear attention (Katharopoulos et al., 2020; Yang et al., 2024), and a recent RAT model (Wei et al., 2025), which inspired our architecture. Especially, RAT chunks the sequence, applies a forget-gate-like recurrence over attention keys and values within each chunk, and then performs inter-chunk attention (i.e., dilated attention) on the gated representations. These models typically require retraining for each design configuration to achieve high efficiency and strong performance, which is costly and inflexible across downstream hardware and task requirements.

The second category focuses on inference-time sparsification, where a sparsified attention pattern is applied during inference. Dense pretrained models can often be sparsified into local (Xiao et al., 2023) or importance-based patterns, such as top-k block attention (Tang et al., 2024; Lu et al., 2025), with different strengths. For example, local attention reduces both computational and memory footprints but can be limited in capturing long-range dependencies, whereas importance-based sparsification can better preserve accuracy but may introduce additional overhead. Beyond these options, we find that dense attention fails to adapt to a classic structured pattern: *dilated attention*. Although dilated attention is hardware-friendly and can substantially reduce both FLOPs and KV cache usage while preserving long-range connectivity, sparsifying a dense model into a dilated pattern results in severe performance degradation, even when combined with local attention.

This raises a practical question: can we train a single model once and, at inference time, flexibly enable dilated attention and its hybrids without retraining separate sparse models? To address this, we study dilated attention from both perspectives: comparing it with RAT by training from scratch, and analyzing its sparsification from dense attention. Together, these results show that introducing a separate model, such as recurrence, is important for pretraining and nec-

essary in the inference-time sparsification setting to explicitly construct a complete receptive field for dilated attention. Although RAT itself is a sparse architecture designed for training from scratch and cannot be directly used for sparse inference, we propose **RAT+**, which retains a dense architecture during pretraining and enables flexible sparse inference. To ensure consistent recurrence behavior across different dilation settings, RAT+ adopts an overlapped chunk formulation, which further simplifies to full-sequence recurrence, and incorporates active recurrence learning. In brief, dilated attention requires an explicit mechanism to construct a complete receptive field; recurrence provides it.

In experiments, we demonstrate that a pretrained RAT+ can be adapted to different dilated attention configurations (with optional local attention), as well as hybrid variants across layers and heads, using only 1B tokens for resolution adaptation. These variants maintain strong performance on short-context commonsense reasoning tasks (Gao et al., 2024) (e.g., a dilation size of 16 brings 1-point accuracy drop, while allowing for 10× and 20× higher full-model maximum throughput for 1K-token decoding at context lengths of 4K and 16K, respectively), as well as on the LongBench (Bai et al., 2023) benchmark. Moreover, we show that RAT+ performs better in top-k block pattern compared to the standard attention on needle-in-a-haystack (NIAH) tasks in the RULER (Hsieh et al., 2024) benchmark.

Instead of pretraining a sparse model, RAT+ is a dense architecture that enables more flexible inference-time efficiency. Our main contributions include:

1. We study the challenge of dilated attention in both training-from-scratch and inference-time sparsification settings. Based on these findings, we propose a novel dense architecture, RAT+, which incorporates full-sequence recurrence and active recurrence learning.
2. Our proposed RAT+ architecture can be pretrained once and then adapted to different dilation sizes (with an optional local window) and hybrid variants, using only a 1B token for resolution adaptation. Moreover, we find that RAT+ outperforms attention-only models in top-k block attention.
3. We primarily pretrain models on the 1.5B scale on 100B tokens and evaluate different configurations on short-context, long-context, and retrieval-heavy tasks. Further experiments on larger scales, including 2.6B RAT+ models with 100B and 200B tokens, show that larger models exhibit a smaller loss gap between dense and dilated attention, demonstrating the scaling potential of RAT+.

2. Preliminaries

We denote the sequence length with T , dilation size by D , local window size by W , chunk size by L , and the number of

blocks selected in the attention of the top-k block by K . D^\dagger is used to highlight the attention model without recurrence.

We distinguish the size of the chunk from the dilation size below, noting that the original RAT sets $L = D$. Within each chunk, RAT first applies a simple linear recurrence over the attention keys k and values v , which reduces to forget-gate behavior with an input-dependent gate g . For the token at position l ,

$$\begin{aligned}\tilde{v}_l &= g_l \odot \tilde{v}_{l-1} + (1 - g_l) \odot v_l, \\ \tilde{k}_l &= g_l \odot \tilde{k}_{l-1} + (1 - g_l) \odot k_l.\end{aligned}\tag{1}$$

It has $\mathcal{O}(1)$ FLOPs and KV cache, and can be implemented through a one-step update in decoding and parallel scan in prefilling and training. Then, for a token at position d in dilation block b , dilated attention is applied over the gated keys and values:

$$y_{b,d} = f([\mathbf{q}_{b,d} \tilde{\mathbf{K}}_{:, -1}^\top; \mathbf{q}_{b,d} \tilde{\mathbf{k}}_{b,d}^\top])[\tilde{\mathbf{V}}_{:, -1}; \tilde{v}_{b,d}],\tag{2}$$

corresponding to the pattern shown in Fig. 1(c), which reduces both FLOPs and the KV cache size by a factor of D . We do not consider the sliding variant, as it reduces parallelism during prefilling and training, and has to keep the full KV cache for decoding.

3. Motivation for recurrence

We analyze how the simple recurrence Eq. (1) enables effective dilated attention by bridging disconnected attention patterns. We study this from both the training-from-scratch and the inference-time sparsification perspectives.

Training-from-scratch We find that the recurrence used in RAT plays a critical role in its subsequent inter-chunk attention (which corresponds to dilated attention), and we attribute this to its ability to provide a complete layer-wise receptive field.

To demonstrate this, we conducted experiments in Table 1 comparing dilated attention with and without recurrence, as well as with optional local attention. We observe that dilated attention without recurrence fails to properly optimize and converges to suboptimal plateaus during training, as expected given the disconnected attention graph. While adding local attention links neighboring tokens to form a conceptually connected attention graph, it must also serve a distinct primary role: selectively aggregating fine-grained information within the local window for the current token. We hypothesize that this dual responsibility limits the ability of local attention to reliably support effective graph connectivity in dilated attention. In contrast, recurrence explicitly and independently provides such support. Moreover, even dense attention benefits from the introduction of recurrence, as shown in the last block of Table 1.

Table 1. Results of training 1B-parameter models on 100B tokens from scratch, with or without the simple recurrence. All models are equipped with output gating (denoted as ogate below), which has been shown to be effective in prior work (Hua et al., 2022; Qiu et al., 2025). Perplexity (PPL) is measured on a held-out 0.5B-token validation set with a 4K sequence length, and Avg. CSR denotes the average across six commonsense reasoning tasks. Note that local attention typically achieves strong performance on short-context tasks while 7.96 at $D^\dagger = 64, W = 64$ is a high PPL. See Table 9 for implementation details and full results.

Model	Val PPL T = 4096	Avg. CSR T ≤ 300
dilated attention ($D^\dagger = 8$)	43.89	Fail
RAT (L = 8, D = 8)	7.52	57.54
dilated attention ($D^\dagger = 16$)	63.94	Fail
RAT (L = 16, D = 16)	7.60	56.99
dilated attention ($D^\dagger = 64, W = 64$)	7.96	57.40
RAT (L = 64, D = 64, W = 64)	7.63	58.74
attention	7.44	58.33
attention + recurrence	7.38	58.84
attention - ogate	7.61	57.54
attention - ogate + recurrence	7.52	58.23

Inference-time sparsification Although dense attention models can be sparsified into local attention or importance-driven patterns such as top-k block attention, they do not adapt effectively to dilated attention, even when equipped with local attention, as shown in Table 2. We further apply a light degree of fine-tuning to assess whether this issue can be mitigated.

First, lightly tuning a sparsified dilated attention pattern from a pretrained dense model yields a rapid loss decrease with a small number of tokens, after which the gains become much smaller, leaving a substantial gap relative to training from scratch. We view this initial rapid improvement as a *resolution-adaptation* process when switching from continuous dense attention to dilated connections. This effect is conceptually related to the fine-tuning used when adjusting positional encoding frequencies (Peng et al., 2023b; bloc97, 2023), but is simpler here, as it does not require attention length generalization. Moreover, because local attention in this setting is treated solely as an inference-time configuration and is not explicitly trained to construct a complete receptive field, there remains a clear performance gap relative to the training-from-scratch regime, potentially requiring prolonged, continued pretraining to close.

In general, results from both aspects highlight the importance of explicitly constructing a complete receptive field for dilated attention, for example, via simple recurrence Eq. (1). Although the efficient RAT architecture can address this problem in the pretraining setting, it does not extend directly to the inference-time sparsification regime. Next, we introduce an architecture designed to address this challenge.

Table 2. We tune the pretrained attention model with different numbers of tokens into the sparse variant (four initial tokens have already been added for attention sink (Xiao et al., 2023)) and refer to the initial phase with rapid loss reduction (within a few hundred million tokens) as the resolution adaptation process. After this phase, improvements exist but much slower, as other modules such as local attention or the FFN are required to mitigate the performance gap, often requiring substantially longer retraining to match training-from-scratch (e.g., $D^\dagger = 64, W = 64$ as 7.96 and $D^\dagger = 1$ as 7.44) performance. We also observe that hundreds of millions tokens is enough for RAT+ Fig. 7, though we use 1B tokens in practice to ensure sufficient adaptation.

Val PPL	0	500M	1B	2B	3B
$D^\dagger = 16, W = 16$	11.51	9.54	9.37	9.22	9.11
$D^\dagger = 64, W = 64$	9.20	8.63	8.57	8.51	8.47
$D^\dagger = 4$	4590	43.85	40.71	37.99	36.52

4. RAT+: Dense model for sparse inference

We now propose a simple and novel architecture based on RAT for inference-time sparsification, where a single dense model is trained once (e.g. $D = 1$) and effectively adapted at inference time to different sparse attention patterns, including dilated attention (e.g. $D = 1, 2, 4, 8, 16, 32, 64$).

The RAT architecture is insufficient for this purpose, as it is a sparse design originally developed for training from scratch and obviously lacks the dense attention capability required in $D = 1$. More concretely, the pretraining-free setting requires: (1) dense attention capacity together with a recurrence capacity that can reliably handle sequences of at least length 64 required in $D = 64$; and (2) recurrence outputs follow the consistent distributions across different configurations, so that subsequent dilated attention does not have to cope with mismatched input distributions, which would otherwise hinder effective adaptation.

Overlapped chunk size The RAT architecture sets the chunk size equal to the dilation size. For example, a recurrence trained with length $L = 64$ must be adapted to $L = 4$ when performing inference at $D = 4$. While it can handle shorter sequences, we observe that recurrence outputs at early time steps exhibit substantially different distributions (Fig. 8), making subsequent dilated attention difficult to adapt to this distribution shift. Such discrepancies at initial steps have also been identified as a form of covariate shift in prior work (Cooijmans et al., 2016). Consistently, the ablation results in the first row of Table 10 show that adapting to small chunk sizes, which corresponds to initial time steps, leads to noticeably higher perplexity because of violating requirement (2).

Instead of applying normalization across time steps, which increases complexity and slows training, we use overlapped recurrence chunks with a fixed-length L for each token (i.e., each token is associated with a fixed-length recurrence win-

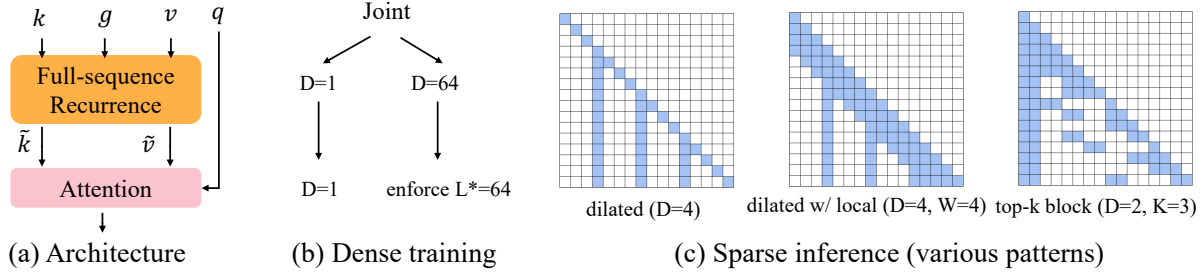


Figure 1. (a) For architectural simplicity, we adopt an extreme overlapped setting, i.e., full-sequence recurrence with $L = T$. (b) Joint training to preserve dense attention capability while enforcing active recurrence learning with desired effective length $L^* = 64$. (c) After pretraining, the resulting model can be efficiently adapted to various sparse inference patterns including effective results on dilated attention (optional local attention), and better performance on top-k block one compared to attention.

dow) throughout training and inference. During evaluation, the dilation size is varied while keeping L fixed (e.g., $L = 64$), satisfying the requirement (2) with the consistent recurrence outputs across different dilation settings.

Active recurrence learning We also need to satisfy requirement (1) by learning both dense attention and recurrence abilities. However, in the current architecture, the overlapped recurrence is hierarchically applied to the attention key and value activations before the scaled dot-product operation. We find that directly training it leads to lazy recurrence learning. Because full-sequence attention already provides complete connectivity, the model can rely on it regardless of the effective range learned by the recurrence. As a result, the recurrence has little incentive to pursue the intended length capability and instead converges to a shorter length that is easier to learn. Empirically, we observe in Table 10 that such models still exhibit high perplexity under sparse inference, though much better than attention.

To guarantee that the overlapped recurrence learns the required length (e.g., 64), we are motivated by the insight in Sec. 3 that a complete receptive field is critical for strong performance. We therefore introduce a stricter training configuration in which acquiring the desired recurrence capability provides a clear advantage over the shorter one. Concretely, we consider the sparse setting $L = 64, D = 64$, where insufficient recurrence capacity directly leads to degraded performance. Based on this, we adopt a simple joint training strategy that updates the model with a sparse case ($L = 64, D = 64$) and a dense case ($L = 64, D = 1$) per batch of data. The sparse case enforces active recurrence learning (ARL), while the dense case preserves sufficient attention capacity, ensuring strong performance in both dense and dilated settings. See Table 10 for a comparison with another training strategy.

Simplification Moreover, active recurrence learning allows us to further simplify the architecture by extending the

overlapped chunk size 64 to the sequence length without performance loss, resulting in a full-sequence recurrence in implementation. This change reduces training to a single parallel forward scan over the sequence and simplifies KV cache management for recurrence. The minimum required recurrence capability (e.g., 64) is then enforced by sparse dilated attention during joint training, while longer-length ability is learned only when favored by the training loss. Consequently, we denote the full-sequence recurrence by $L = T$ and use L^* for the actively enforced recurrence length when they differ. Fig. 6 and Subsec. 5.3 justify the choice of 64 based on the trade-off between the recurrence capacity and the flexibility of the dilation settings.

To conclude, as shown in Table 3, with full-sequence recurrence and active learning, RAT+ achieves dense performance comparable to attention while remaining effective in different dilation settings, with even stronger sparse results than training RAT from scratch, benefiting from dense FLOPs training.

Table 3. PPL performance of adapting different models to different dilation sizes with 1B tokens. Entries in the Train column marked with two settings denote training on both. For attention, we also include two variants trained under the joint training setting similar to RAT+. The failures of RAT at small dilation sizes come from its lack of dense-attention capability and the use of chunk sizes equal to the dilation size. The gray row corresponds to the final RAT+ with full-sequence recurrence ($L = T$) and an active recurrence length of $L^* = 64$.

Model	Train	Inference (D value)						
		1	2	4	8	16	32	64
attention								
-	$D^\dagger = 1$	7.44	17.2	41.0	65.1	87.9	110	129
-	$D^\dagger = 1, W = 64$	7.41	16.7	40.2	64.3	87.2	109	129
-	$D^\dagger = 1, D^\dagger = 64$	7.82	16.2	34.7	53.0	70.9	90	110
RAT ($L = 16$)	$D = 16$	8.41	8.08	7.79	7.64	7.61	7.74	7.93
RAT+								
$L = 64$	$D = 1, D = 64$	7.4	7.42	7.45	7.48	7.52	7.58	7.67
$L = T, L^* = 64$	$D = 1, D = 64$	7.4	7.42	7.45	7.48	7.52	7.58	7.66

5. Experiments

In this section, we first present the performance of RAT+ under various sparse inference patterns, including dilated, hybrid, and top-k block attention. We then report efficiency, scaling, and ablation studies.

5.1. Settings

We primarily pretrain 1.5B-parameter models on 100B tokens from FineWeb-Edu (Penedo et al., 2024), using a context length of 4096. All models use output gating with a corresponding linear projection (Hua et al., 2022; Qiu et al., 2025); RAT+ further includes one extra projection for the recurrence. We leave saving parameters for future work. Full implementation details are provided in the Subsec. A.1.

Unless otherwise specified (e.g., hybrid models), each sparse pattern is applied uniformly across all layers and used for both prefilling and decoding. (1) In **dilated attention with an optional local window**, we additionally add four initial tokens following StreamingLLM (Xiao et al., 2023) for the attention sink problem in both accuracy and efficiency studies. This scheme reduces both FLOPs and KV cache size from $\mathcal{O}(T)$ to $\mathcal{O}(T/D)$ with an optional $\mathcal{O}(W)$. (2) In **hybrid design**, we evaluate the feasibility of hybrid layer-wise or head-wise sparse designs, rather than searching for optimal configurations which depend strongly on properties of the pretrained model (e.g., layer or head sparsifiability and preferred dilation). We leave the optimal choice for future work. (3) **Top-k block attention** selects the most relevant blocks (block size indicated by dilation size D , number K) for each query token and computes attention only for them. We always choose the first and the most recent block, and leave the others to be decided by Quest (Tang et al., 2024) and MoBA (Lu et al., 2025). This scheme does not use adaptation and is applied directly. Note that it is less efficient than dilated or local attention (e.g., no KV cache reduction and extra block scoring).

5.2. Main results

Does RAT+ preserve dense performance and enable stable dilation? As shown in Table 3, RAT+ preserves perplexity for the dense pattern compared to attention-only models trained under the same FLOPs budget. Also, RAT+ remains stable across dilation settings, whereas attention-only models exhibit extremely high perplexity when directly sparsified into dilated attention (e.g., over 100 at $D = 64$).

We further evaluate the feasibility of dilated inference on downstream commonsense reasoning benchmarks (Gao et al., 2024) for general language understanding (Table 4). As shown in the table, $D = 16$ achieves nearly the same average accuracy as dense attention ($D = 1$), and $D = 64$ incurs only about a 2-point drop, while reducing temporal-mixing

Table 4. Performance of RAT+ on common-sense reasoning tasks. Models in the first two blocks are obtained by adapting pretrained dense models with a lightweight adaptation stage of 1B tokens, while models in the third block are trained from scratch. Task definitions and evaluation metrics follow (Yang et al., 2024), and the results for the last two models are taken from (Dao & Gu, 2024; Yang et al., 2024). We report temporal-mixing FLOPs per token for each configuration. All tasks involve short contexts with $T \leq 300$; in particular, LMB. and Wino. have even shorter contexts. Thus large dilation settings almost reduce to a single recurrence. The $D = 128$ is enabled via length generalization of the recurrence.

Model	FLOPs $T \leq 300$	ARC-C acc.n	ARC-E acc	Hella. acc.n	LMB. acc	PIQA acc	Wino. acc	Avg. -
RAT+ ($L^* = 64$)								
$D = 1$	T	40.78	73.23	59.81	50.34	73.56	57.54	59.21
$D = 2$	T/2	41.47	73.23	59.55	50.36	73.34	56.51	59.08
$D = 4$	T/4	41.21	72.98	59.46	49.18	73.39	56.75	58.83
$D = 8$	T/8	40.96	72.98	59.09	48.52	73.23	54.70	58.25
$D = 16$	T/16	40.44	73.06	58.89	47.72	72.85	55.41	58.06
$D = 32$	T/32	40.53	73.19	58.20	45.74	72.85	56.83	57.89
$D = 64$	T/64	39.76	72.90	57.93	44.05	72.91	57.22	57.46
$D = 128$	T/128	39.59	73.19	57.37	41.8	72.91	57.69	57.09
attention								
$D^\dagger = 1$	T	40.1	71.84	58.5	49.95	72.42	57.14	58.33
$D^\dagger = 16$	T/16	23.04	35.23	28.58	0.99	56.53	51.22	32.60
RAT								
Mamba2	T/16	39.76	72.6	56.95	46.03	72.14	54.46	56.99
GatedDeltaNet	256	37.88	72.47	55.67	45.66	71.87	55.24	56.47
	288	38.39	71.21	55.76	46.65	72.25	57.45	56.95

FLOPs by $64\times$.

Table 5. LongBench performance of different sparse inference patterns. Due to space constraints, other less informative tasks are deferred to Appendix Table 12 (e.g., similar performance on LCC or uniformly low scores on MusiQue). Since LongBench is prompt-heavy where pretrained-only models can be sensitive to, we focus on overall trends. Moreover, for hybrid patterns, we present several representative examples to demonstrate feasibility rather than identifying optimal designs, as the optimal configuration depends on properties of the pretrained model (e.g., layer-wise sparsification preferences). NQA: NarrativeQA; MF: MultiField-en; HQA: HotpotQA; 2WQA: 2WikiMultihopQA; RBP: RepoBench-P.

RAT+ ($T = 4096, L^* = 64$)	NQA	Qasper	MF	HQA	2WQA	RBP	Avg.
Dilated (opt. local)							
$D = 1$	13.87	15.59	27.45	15.38	17.53	26.42	19.37
$D = 2$	14.23	15.92	25.86	16.13	16.92	24.83	18.98
$D = 4$	13.89	14.65	24.24	14.82	16.55	24.74	18.15
$D = 8$	14.13	14.37	26.06	14.7	16.26	24.37	18.32
$D = 16$	14.72	14.54	25.99	14.68	17.4	23.68	18.50
$D = 32$	12.9	13.81	25.16	13.38	17.24	21.98	17.41
$D = 64$	13.89	13.99	21.57	13.18	14.7	22.03	16.56
$D = 128$	12.76	12.35	21.32	12.02	16.96	22.65	16.34
$D = 16, W = 256$	14.06	13.69	24.75	14.15	17.9	27.49	18.67
$D = 8, W = 512$	14.3	15.23	24.44	15.79	17.57	26.57	18.98
$W = 1024$ (StreamingLLM)	11.7	14.12	21.68	14.68	13.77	26.09	17.01
$W = 256$ (StreamingLLM)	11.34	12.18	19.38	12.84	15.55	26.22	16.25
Hybrid (layer-wise)							
$D = 16$ (even layers) $W = 1024$	12.97	14	22.01	13.63	17.51	26.01	17.69
$D = 1$ (0, 12) $D = 16, W = 256$	13.46	14.3	26.53	15.08	16.36	26.39	18.69
Hybrid (head-wise)							
$D = 1$ (first two) $D = 4$	14.54	15.59	25.56	17.31	18.86	23.73	19.27
NTK extended ($T = 16384$)							
$D = 1$	14.74	18.5	31.27	16.83	16.52	25.25	20.52
$D = 4$	14.34	17.39	30.96	15.99	17.9	24.58	20.19

Does RAT+ support various sparse inference patterns?

We then evaluate a wider range of efficient schemes on LongBench (Bai et al., 2023) in Table 5, which consists of long-context tasks and is therefore suitable for studying

sparse inference patterns. A key finding is that different downstream tasks favor different sparsification strategies, supporting our train-dense, adapt-sparse paradigm. For example, RBP task largely prefers the local attention pattern rather than the dilated one. By combining them within each layer or in different layers can recover the performance back to 26. Also, inserting a small number of dense layers can benefit tasks such as MF.

For hybrid sparse inference patterns, we emphasize that our goal is to demonstrate the feasibility, rather than to identify optimal hybrid designs. For example, the hybrid configuration of $D = 16$ interleaved with $W = 1024$ achieves intermediate performance, with clear improvements over local-window-only models (e.g., +4 points on 2WQA), but does not outperform the dilated one on average. This is because, *unlike training-from-scratch regime where functionality can be freely allocated across modules during optimization, inference-time hybrid configurations are constrained by the pretrained specialization of layers and heads*. Different components may vary in how amenable they are to sparsification, as well as in the dilation or window sizes at which they operate most effectively. We leave the search of optimal hybrid sparse patterns to future work.

More results include length generalization with the NTK-based RoPE scaling method (bloc97, 2023), which allows us to either increase FLOPs proportionally or keep them unchanged by expanding the dilation size when extending to longer sequence lengths, as well as additional NIAH results in Appendix Table 13.

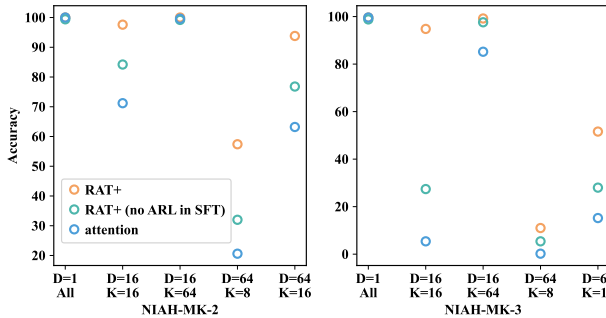


Figure 2. Results of top-k block attention with block size D and number of selected blocks K on the hard NIAH-MK-2 and NIAH-MK-3 tasks from the RULER benchmark with $T = 4096$. RAT+ (no ARL in SFT) means disabling active recurrence learning during the SFT, which further demonstrates the benefit of the recurrence. More results include remaining tasks in Table 14, MoBA-style top-k block attention in Table 15, dilated attention in Table 13

Does recurrence help beyond dilation (top-k block)? Beyond dilated attention, we also evaluate performance when directly sparsified to top-k block attention in Fig. 2, Table 14 and Table 15. Interestingly, we find that top-k block attention performs substantially better when sparsified from

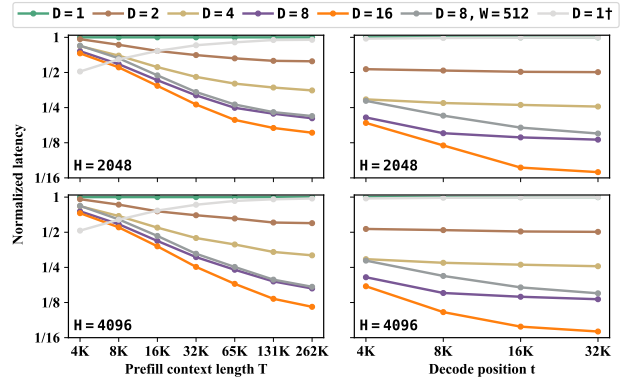


Figure 3. Efficiency results of the temporal-mixing operator on a single GH200 GPU, covering both prefilling and decoding scenarios with hidden dimension H . Prefilling latency is measured on sequences of 262K tokens. Decoding latency is measured for 256 or 128 batches of tokens for the two hidden dimensions, respectively; the baseline runs out of memory beyond 32K tokens. We use FlexAttention (Dong et al., 2024) for prefilling (with $D = 1$ reducing to FlashAttention), and FlashAttention (Dao et al., 2022) for decoding. Recurrence is implemented by associative scan in PyTorch for prefilling and a simple step update for decoding. Due to space constraints, additional results are reported in Appendix D.

RAT+ than from attention-only models. We hypothesize that recurrence encourages token representations to better reflect the content of their block, so that block selection algorithms (e.g., min/max or mean pooling) can capture this information more effectively. This in turn leads to more accurate block scoring and improves final performance.

We use the NIAH tasks from the RULER benchmark to illustrate this effect. These retrieval-heavy tasks are particularly sensitive to block selection quality. To exclude prompt sensitivity in pretrained-only models, we apply a supervised fine-tuning (SFT) stage to make models faithfully follow instructions before all evaluations. In Fig. 2, all dense configurations achieve perfect accuracy, whereas sparse variants from attention-only models suffer significant degradation. Compared to them, sparse variants from RAT+ maintain much higher accuracy (e.g., 93.8 vs. 63.2 on NIAH-MK-2 at $D = 64, K = 16$). Moreover, enabling active recurrence learning during SFT by jointly tuning the dense and corresponding dilated variants is critical, as it allows recurrence to actively absorb task-specific information. Consistent improvements across other NIAH tasks and an additional top-k block attention method are reported in the Appendix C. We also present an interesting finding there when comparing these results with those of dilated attention.

What are the actual latency/throughput wins? First, for prefilling latency, linear projections dominate at short sequence lengths, while the temporal-mixing operator for attention becomes the main bottleneck at longer contexts. At 4K length, full-sequence recurrence incurs latency com-

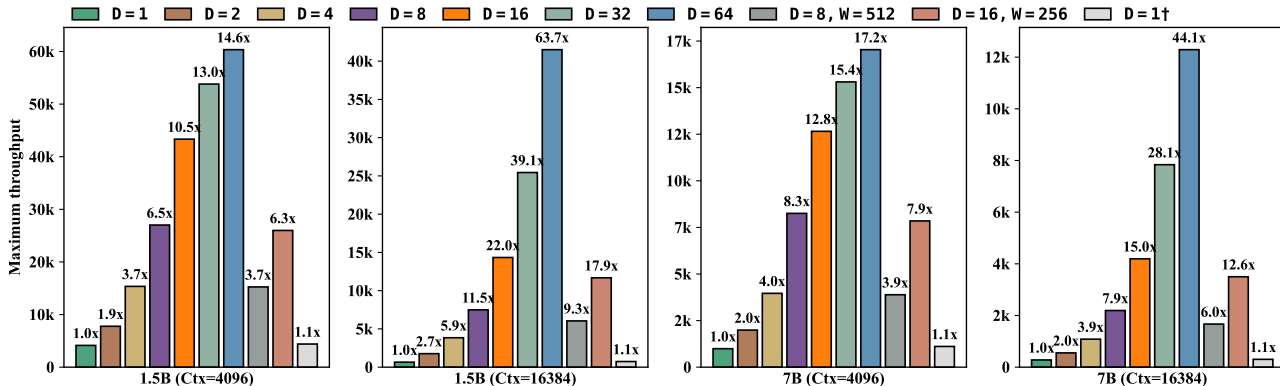


Figure 4. Maximum decoding throughput (tokens/sec) of the full 1.5B and 7B models for decoding 1024 tokens, measured at context lengths of 4096 and 16384, corresponding to prefilling lengths of 3072 and 15360 tokens, respectively.

parable to well-optimized FlashAttention, but this overhead becomes relatively minor once linear projections are included (Table 17) or when sequence lengths further increase. At long sequence lengths, the RAT+ operator with $D = 16$ achieves up to $6.3\times$ and $8.5\times$ speedups for hidden dimensions 2048 and 4096 at 262K prefilling length, respectively. When benchmarking the temporal-mixing block with linear layers included, where the extra recurrence projection and shared projection overhead reduce the measured speedup, we still obtain $5.5\times$ and $6\times$ improvements over the attention block, as shown in Table 17 and Table 19.

For decoding latency (see Table 18 and Table 20), temporal-mixing operator dominates even when generating tokens at moderate positions such as 4K. We found that when GPU resources are sufficiently utilized (e.g., larger batch sizes, hidden dimensions, or longer sequence), RAT+ can yield wall-clock speedups close to the dilation factor (e.g., $14\times$ for $D = 16$) at the operator level. In this regime, linear projections with the extra one contribute relatively little to decoding latency, so the block-level speedups closely match those observed at the operator level.

Finally, in Fig. 4, we benchmark end-to-end throughput on full models with 1.5B and 7B parameters, where jointly reducing KV cache size and FLOPs, $D = 64$ can achieve over $60\times$ and $40\times$ better throughput respectively.

Does the model scale with size? We further investigate scaling up and down to demonstrate that the proposed RAT+ architecture generalizes across different model sizes and datasets. For the smaller scale, we train a 200M-parameter model on the PG19 book dataset (Rae et al., 2019), with detailed results reported in the Table 11. For the larger scale, we scale the 1.5B model up to 2.6B parameters and optionally consider training with more tokens. Interestingly, as we scale the model from 1.3B to 2.6B, the performance gap between sparse and dense attention (e.g., $D = 64$ and $D = 1$

in Fig. 5) becomes smaller. Downstream evaluations on 2.6B models are provided in the Table 16). We attribute this to the increased capacity of recurrence with a larger hidden dimension, which better supports modeling 64 length.

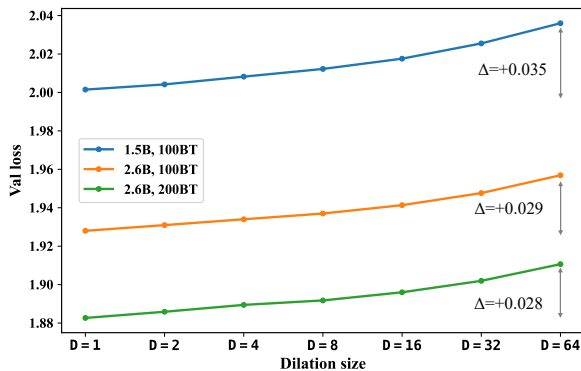


Figure 5. Scaling-up experiments. We report validation loss on a held-out 0.5B-token subset of the FineWeb dataset to illustrate the loss gap between dense and sparse configurations.

5.3. Design choices

As mentioned in Sec. 4, the ablation studies for the two techniques are reported in Table 10. Here, we briefly discuss other design choices.

Why recurrence? We adopt recurrence primarily for its simplicity compared to MLPs, convolutions, attention, and linear attention. In contrast, these alternatives are heavier and more complex, which may introduce optimization difficulties in this hierarchical architecture. A second motivation is input-dependent temporal modeling. The recurrence employed here uses input-conditioned forget gates, which adapt to the dynamics of text sequences. MLPs are not time-variant, and both convolutions and attention require interactions with all tokens within the chunk, and thus would require more parameters under the overlapped chunk size.

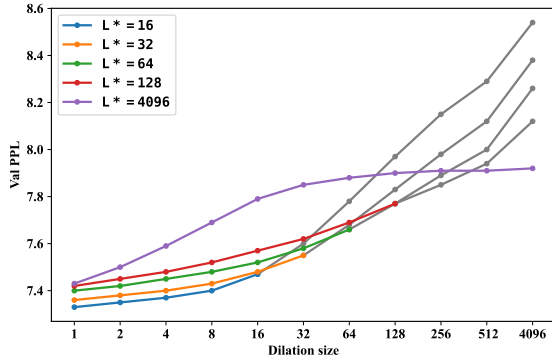


Figure 6. Choice of $L = 64$. $L^* = 16$ means $D = 1$ and $D = 16$ joint training to enable 16 length capability for recurrence. Different performance on $D = 1$ comes from different training FLOPs and different recurrence abilities in capturing the corresponding length. Grey points indicate recurrence length generalization.

How recurrence? Our design follows RAT (Wei et al., 2025), which applies recurrence to attention keys and values in a hierarchical manner. Similar designs have also appeared in recent work (Zhang et al., 2024; Yuan et al., 2025), using different modules and targeting different objectives. We evaluate other variants in Appendix Table 11, and the adopted design consistently performs best.

Choice of $L = 64$. This is an empirical choice in RAT+. Intuitively, $L = 64$ is not a large sequence length, and recurrence can handle it reliably without suffering from memory degradation in long-context modeling. At the same time, it is not a small value: by covering dilation up to 64, it provides sufficient flexibility for choosing dilation sizes and constructing hybrid models with high speed-up. Moreover, it is safer for length generalization compared to $L = 16$. We also ablate other active recurrence lengths, as shown in Fig. 6. Taking these trade-offs and empirical results into account, we finally choose $L = 64$ in this paper.

5.4. Further analyses

Comparison with GQA and MQA Similar to RAT+, grouped-query attention (GQA) and multi-query attention (MQA) (Ainslie et al., 2023; Shazeer, 2019) also reduce the KV cache size, but in orthogonal ways. RAT+ leverages recurrence to compress the *key* and *value* activations within dilation, whereas GQA and MQA reduce the KV cache by sharing projection heads across tokens. We report comparisons in Table 6. Here we mainly highlight the flexibility of RAT+. First, it only requires pretraining a single dense model, while GQA and MQA use separate training from scratch. Second, RAT+ can combine dilated attention with a local window to preserve the original KV cache size in the local region, thereby retaining local information, which is not achievable with GQA.

Table 6. Comparison with GQA and MQA on the 1.5B model scale, where N_{kv} denotes the number of *key* or *value* heads. Since RAT+ is trained with joint training, we also adopt joint training for GQA/MQA for a fair comparison. We use $D^\dagger = 1$ and $W = 64$ for them because as shown in Table 3, using dilated attention without a recurrence leads to higher perplexity. Here, we highlight the flexibility of RAT+, which only requires pretraining once and can optionally avoid compressing the local window.

Method	Config	Cache reduction	Val PPL
GQA / MQA	$N_{kv} = 1$	$16\times$	7.62
	$N_{kv} = 2$	$8\times$	7.68
	$N_{kv} = 4$	$4\times$	7.53
RAT+	$D = 16$	$16\times$	7.52
	$D = 8$	$8\times$	7.48
	$D = 4$	$4\times$	7.45

Table 7. Validation perplexity of RAT+ when trained without positional encoding (NoPE). The validation perplexity (PPL) is comparable to, or slightly better than, the RoPE baseline.

PE	Inference (D value)						
	1	2	4	8	16	32	64
RoPE	7.40	7.42	7.45	7.48	7.52	7.58	7.66
NoPE	7.40	7.42	7.45	7.47	7.50	7.55	7.63

Performance without positional encoding (NoPE) While we use RoPE in the experiments above, we also investigate the NoPE setting. Surprisingly, the training curves remain stable under the same optimization hyperparameters and achieve comparable or slightly better perplexity when positional encodings are removed, as shown in Table 7. We hypothesize that this is enabled by joint training. NoPE assumes that positional information can be implicitly inferred from causal masks and attention patterns (Kazemnejad et al., 2023). Then, in RAT+, with joint training, the sparse configuration $D = 64$ effectively reduces the attention span to 64 tokens under a context window of 4K. This shorter effective context makes it easier to leverage positional cues from the causal masks, compared to directly learning positional structure of 4K context length. In contrast, directly training attention-only models with full NoPE layers often results in slightly worse training loss, as also reported in prior work (Haviv et al., 2022; Yang et al., 2025).

Combination of top-k block attention with dilation In the previous subsection, we showed that RAT+ supports dilated inference and improves the performance of top-k block attention. One natural question is how these two mechanisms compare and whether they can be combined. The comparison results with some analyses are reported in Appendix C on the Ruler benchmark. Here we focus on the latter question: using them together within the same layer or head, where top-k block attention provides fine-grained focus on selected positions and dilated attention supplies coarse-grained information for the remaining blocks. We

find that this combination works effectively. In this experiment, we use a relatively large block size ($D = 64$). Larger blocks reduce the FLOPs required for block scoring and improve memory locality, but may lead to lower performance (e.g., RAT+ achieves perfect results with a block size of 16). As shown in Table 8, providing additional coarse-grained block-level information significantly improves performance—from 57.4 to 97.4 on NIAH-MK-2 and from 11.0 to 79.6 on NIAH-MK-3 when selecting 8 blocks.

Table 8. Performance of combining dilated and top-k block attention (e.g., $D = 64 \mid D = 64, K = 16$), where each token attends to every token within K critical blocks, while also attending to other blocks through compressed information provided by dilation. Here we focus on the challenging setting with a large block size of 64 for the top-k block pattern.

Model	NIAH-MK-2	NIAH-MK-3
$D = 64, K = 8$	57.4	11.0
$D = 64 \mid D = 64, K = 8$	97.4	79.6
$D = 64, K = 16$	93.8	51.6
$D = 64 \mid D = 64, K = 16$	99.2	97.0

6. Related works

6.1. Efficient pretrained architectures

Many efficient architectures are designed and trained from scratch as alternatives to dense attention, including structured sparse patterns such as sliding-window and dilated attention (Ding et al., 2023; Beltagy et al., 2020; Zaheer et al., 2020; Hassani & Shi, 2022; Liu et al., 2021; Co-here et al., 2025; Yuan et al., 2025). Dilated-only schemes often require careful rate compositions to ensure full receptive fields and can be harder to optimize than dense models (Fournier et al., 2023; Hamaguchi et al., 2018). Other recent approaches build on state space models and linear attention (Gu & Dao, 2023; Dao & Gu, 2024; Yang et al., 2024; Zhang et al., 2024; Peng et al., 2023a; Katharopoulos et al., 2020; Sun et al., 2023; Orvieto et al., 2023), exploring the duality between linear recurrence and linear attention. A closely related architecture is RAT (Wei et al., 2025), which hierarchically combines recurrence and attention and can interpolate between them. Our analysis builds upon RAT, motivated by the observation that its inter-chunk attention mechanism is indeed dilated attention and yields strong training performance with recurrence. Finally, a key limitation of such efficient pretrained architectures is that they typically require training from scratch for each configuration (e.g., dilation size in (Beltagy et al., 2020) or chunk size in RAT), which largely reduces inference-time flexibility across different task preferences and efficiency budgets.

6.2. Sparse inference for attention models

Many works also study inference-time sparsification of standard attention, motivated by the sparsity of attention maps.

One direction emphasizes local attention (Xiao et al., 2023; Han et al., 2024) and its hybrids (Fu et al., 2024; Xiao et al., 2024b), while another identifies important tokens or blocks for each query token. Such importance-driven methods have been explored for both prefilling (Jiang et al., 2024; Lu et al., 2025; Lai et al., 2025) and decoding (Tang et al., 2024; Zhang et al., 2023; Lin et al., 2025; Xiao et al., 2024a; Zhang et al., 2025; Oren et al., 2024; Li et al., 2024). Liu et al. (2025) additionally applies continued pretraining to train a dedicated indexer. While sparsifying dense attention into these patterns is often effective, we explore the case of dilated attention, which dense pretrained models fail severely. We highlight it as an important structured pattern for its long-range connections beyond local-window schemes and its clean reductions in both FLOPs and KV cache size compared to most importance-driven approaches.

7. Conclusion and Future work

RAT+ points to a promising direction for efficiency: designing dense architectures that retain full dense capability while supporting a broader set of sparse inference patterns, rather than training separate sparse architectures from scratch. Large-scale experiments demonstrate the effectiveness of full-sequence recurrence and active recurrence learning for supporting dilated inference, highlighting RAT+’s potential for future language model development.

Limitations and Future work As mentioned earlier, the efficiency of RAT+ could be further improved with dedicated CUDA kernels. Specialized kernels may also support more diverse sparse patterns, such as combining top-k block attention with dilated attention or using different dilation or window sizes across heads. From an inference perspective, identifying optimal sparse configurations is another interesting direction. Extending RAT+ to larger-scale settings and other modalities also presents promising opportunities. In addition, aspects such as GQA/MQA and NoPE discussed in Subsec. 5.4 merit further investigation.

RAT+ may also benefit several additional scenarios. First, it could be useful in tokenizer-free settings with byte-level inputs, where hierarchical representations are desirable. Dilation naturally controls attention granularity: early layers with small dilation capture fine-grained units such as bytes or words, while deeper layers with larger dilation model higher-level structures such as phrases or sentences more efficiently. Second, RAT+ may benefit parallel-style sampling for reasoning. For example, dilated attention can be used during the exploration phase for fast sampling, after which the model switches to the dense version to generate the final outputs with higher accuracy. This may be feasible because we found that the sparse and dense versions produce highly similar outputs as they’re derived from the same dense checkpoint.

Impact Statement

This paper presents work whose goal is to advance the field of Machine Learning by improving the efficiency of language models. There are many potential societal consequences of language modeling research, none of which we feel must be specifically highlighted here.

Acknowledgements

We sincerely thank the Swiss AI Initiative and the Swiss National Supercomputing Centre (CSCS) for supporting this work through grants under project IDs a-infra01 and a109. We extend our appreciation to Karin Getaz for administrative support.

References

- Ainslie, J., Lee-Thorp, J., De Jong, M., Zemlyanskiy, Y., Lebrón, F., and Sanghai, S. Gqa: Training generalized multi-query transformer models from multi-head checkpoints. In *Proceedings of the 2023 Conference on Empirical Methods in Natural Language Processing*, pp. 4895–4901, 2023.
- Bai, Y., Lv, X., Zhang, J., Lyu, H., Tang, J., Huang, Z., Du, Z., Liu, X., Zeng, A., Hou, L., et al. Longbench: A bilingual, multitask benchmark for long context understanding. *arXiv preprint arXiv:2308.14508*, 2023.
- Beltagy, I., Peters, M. E., and Cohan, A. Longformer: The long-document transformer. *arXiv preprint arXiv:2004.05150*, 2020.
- Bi, X., Chen, D., Chen, G., Chen, S., Dai, D., Deng, C., Ding, H., Dong, K., Du, Q., Fu, Z., et al. Deepseek llm: Scaling open-source language models with longtermism. *arXiv preprint arXiv:2401.02954*, 2024.
- bloc97. NTK-Aware Scaled RoPE allows LLaMA models to have extended (8k+) context size without any fine-tuning and minimal perplexity degradation, 2023.
- Cohere, T., Ahmadian, A., Ahmed, M., Alammari, J., Alizadeh, M., Alnumay, Y., Althammer, S., Arkhangorodsky, A., Aryabumi, V., Aumiller, D., et al. Command a: An enterprise-ready large language model. *arXiv preprint arXiv:2504.00698*, 2025.
- Cooijmans, T., Ballas, N., Laurent, C., Gülçehre, Ç., and Courville, A. Recurrent batch normalization. *arXiv preprint arXiv:1603.09025*, 2016.
- Dao, T. and Gu, A. Transformers are ssms: Generalized models and efficient algorithms through structured state space duality. *arXiv preprint arXiv:2405.21060*, 2024.
- Dao, T., Fu, D., Ermon, S., Rudra, A., and Ré, C. Flashattention: Fast and memory-efficient exact attention with io-awareness. *Advances in neural information processing systems*, 35:16344–16359, 2022.
- Ding, J., Ma, S., Dong, L., Zhang, X., Huang, S., Wang, W., Zheng, N., and Wei, F. Longnet: Scaling transformers to 1,000,000,000 tokens. *arXiv preprint arXiv:2307.02486*, 2023.
- Dong, J., Feng, B., Guessous, D., Liang, Y., and He, H. Flex attention: A programming model for generating optimized attention kernels. *arXiv preprint arXiv:2412.05496*, 2024.
- Fournier, Q., Caron, G. M., and Aloise, D. A practical survey on faster and lighter transformers. *ACM Computing Surveys*, 55(14s):1–40, 2023.
- Fu, T., Huang, H., Ning, X., Zhang, G., Chen, B., Wu, T., Wang, H., Huang, Z., Li, S., Yan, S., et al. Moa: Mixture of sparse attention for automatic large language model compression. *arXiv preprint arXiv:2406.14909*, 2024.
- Gao, L., Tow, J., Abbasi, B., Biderman, S., Black, S., DiPofi, A., Foster, C., Golding, L., Hsu, J., Le Noac’h, A., Li, H., McDonell, K., Muennighoff, N., Ociepa, C., Phang, J., Reynolds, L., Schoelkopf, H., Skowron, A., Sutawika, L., Tang, E., Thite, A., Wang, B., Wang, K., and Zou, A. The language model evaluation harness, 07 2024. URL <https://zenodo.org/records/12608602>.
- Gu, A. and Dao, T. Mamba: Linear-time sequence modeling with selective state spaces. *arXiv preprint arXiv:2312.00752*, 2023.
- Hamaguchi, R., Fujita, A., Nemoto, K., Imaizumi, T., and Hikosaka, S. Effective use of dilated convolutions for segmenting small object instances in remote sensing imagery. In *2018 IEEE winter conference on applications of computer vision (WACV)*, pp. 1442–1450. IEEE, 2018.
- Han, C., Wang, Q., Peng, H., Xiong, W., Chen, Y., Ji, H., and Wang, S. Lm-infinite: Zero-shot extreme length generalization for large language models. In *Proceedings of the 2024 Conference of the North American Chapter of the Association for Computational Linguistics: Human Language Technologies (Volume 1: Long Papers)*, pp. 3991–4008, 2024.
- Hassani, A. and Shi, H. Dilated neighborhood attention transformer. *arXiv preprint arXiv:2209.15001*, 2022.
- Haviv, A., Ram, O., Press, O., Izsak, P., and Levy, O. Transformer language models without positional encodings still learn positional information. In *Findings of the Association for Computational Linguistics: EMNLP 2022*, pp. 1382–1390, 2022.

- Hsieh, C.-P., Sun, S., Krizan, S., Acharya, S., Rekish, D., Jia, F., Zhang, Y., and Ginsburg, B. Ruler: What’s the real context size of your long-context language models? *arXiv preprint arXiv:2404.06654*, 2024.
- Hua, W., Dai, Z., Liu, H., and Le, Q. Transformer quality in linear time. In *International conference on machine learning*, pp. 9099–9117. PMLR, 2022.
- Jacob, B., Kligys, S., Chen, B., Zhu, M., Tang, M., Howard, A., Adam, H., and Kalenichenko, D. Quantization and training of neural networks for efficient integer-arithmetic-only inference. In *Proceedings of the IEEE conference on computer vision and pattern recognition*, pp. 2704–2713, 2018.
- Jiang, H., Li, Y., Zhang, C., Wu, Q., Luo, X., Ahn, S., Han, Z., Abdi, A. H., Li, D., Lin, C.-Y., et al. Minference 1.0: Accelerating pre-filling for long-context llms via dynamic sparse attention. *Advances in Neural Information Processing Systems*, 37:52481–52515, 2024.
- Jordan, K. Muon: An optimizer with momentum and normalization. <https://kellerjordan.github.io/posts/muon/>, 2023. Accessed: 2026-01-26.
- Katharopoulos, A., Vyas, A., Pappas, N., and Fleuret, F. Transformers are rnns: Fast autoregressive transformers with linear attention. In *International conference on machine learning*, pp. 5156–5165. PMLR, 2020.
- Kazemnejad, A., Padhi, I., Natesan Ramamurthy, K., Das, P., and Reddy, S. The impact of positional encoding on length generalization in transformers. *Advances in Neural Information Processing Systems*, 36:24892–24928, 2023.
- Lai, X., Lu, J., Luo, Y., Ma, Y., and Zhou, X. Flex-prefill: A context-aware sparse attention mechanism for efficient long-sequence inference. *arXiv preprint arXiv:2502.20766*, 2025.
- Li, Y., Huang, Y., Yang, B., Venkitesh, B., Locatelli, A., Ye, H., Cai, T., Lewis, P., and Chen, D. Snapkv: Llm knows what you are looking for before generation. *Advances in Neural Information Processing Systems*, 37:22947–22970, 2024.
- Lin, C., Tang, J., Yang, S., Wang, H., Tang, T., Tian, B., Stoica, I., Han, S., and Gao, M. Twilight: Adaptive attention sparsity with hierarchical top- p pruning. *arXiv preprint arXiv:2502.02770*, 2025.
- Liu, A., Mei, A., Lin, B., Xue, B., Wang, B., Xu, B., Wu, B., Zhang, B., Lin, C., Dong, C., et al. Deepseek-v3. 2: Pushing the frontier of open large language models. *arXiv preprint arXiv:2512.02556*, 2025.
- Liu, Z., Lin, Y., Cao, Y., Hu, H., Wei, Y., Zhang, Z., Lin, S., and Guo, B. Swin transformer: Hierarchical vision transformer using shifted windows. In *Proceedings of the IEEE/CVF international conference on computer vision*, pp. 10012–10022, 2021.
- Lu, E., Jiang, Z., Liu, J., Du, Y., Jiang, T., Hong, C., Liu, S., He, W., Yuan, E., Wang, Y., et al. Moba: Mixture of block attention for long-context llms. *arXiv preprint arXiv:2502.13189*, 2025.
- Milakov, M. and Gimelshein, N. Online normalizer calculation for softmax. *arXiv preprint arXiv:1805.02867*, 2018.
- Oren, M., Hassid, M., Yarden, N., Adi, Y., and Schwartz, R. Transformers are multi-state rnns. *arXiv preprint arXiv:2401.06104*, 2024.
- Orvieto, A., Smith, S. L., Gu, A., Fernando, A., Gulcehre, C., Pascanu, R., and De, S. Resurrecting recurrent neural networks for long sequences. In *International Conference on Machine Learning*, pp. 26670–26698. PMLR, 2023.
- Penedo, G., Kydlíček, H., Lozhkov, A., Mitchell, M., Raffel, C. A., Von Werra, L., Wolf, T., et al. The fineweb datasets: Decanting the web for the finest text data at scale. *Advances in Neural Information Processing Systems*, 37: 30811–30849, 2024.
- Peng, B., Alcaide, E., Anthony, Q., Albalak, A., Arcadinho, S., Biderman, S., Cao, H., Cheng, X., Chung, M., Grella, M., et al. Rwkv: Reinventing rnns for the transformer era. *arXiv preprint arXiv:2305.13048*, 2023a.
- Peng, B., Quesnelle, J., Fan, H., and Shippole, E. Yarn: Efficient context window extension of large language models. *arXiv preprint arXiv:2309.00071*, 2023b.
- Qiu, Z., Wang, Z., Zheng, B., Huang, Z., Wen, K., Yang, S., Men, R., Yu, L., Huang, F., Huang, S., et al. Gated attention for large language models: Non-linearity, sparsity, and attention-sink-free. *arXiv preprint arXiv:2505.06708*, 2025.
- Rae, J. W., Potapenko, A., Jayakumar, S. M., Hillier, C., and Lillicrap, T. P. Compressive transformers for long-range sequence modelling. *arXiv preprint*, 2019. URL <https://arxiv.org/abs/1911.05507>.
- Shazeer, N. Fast transformer decoding: One write-head is all you need. *arXiv preprint arXiv:1911.02150*, 2019.
- Su, J., Ahmed, M., Lu, Y., Pan, S., Bo, W., and Liu, Y. Roformer: Enhanced transformer with rotary position embedding. *Neurocomputing*, 568:127063, 2024.

- Sun, Y., Dong, L., Huang, S., Ma, S., Xia, Y., Xue, J., Wang, J., and Wei, F. Retentive network: A successor to transformer for large language models. *arXiv preprint arXiv:2307.08621*, 2023.
- Tang, J., Zhao, Y., Zhu, K., Xiao, G., Kasikci, B., and Han, S. Quest: Query-aware sparsity for efficient long-context llm inference. *arXiv preprint arXiv:2406.10774*, 2024.
- Vaswani, A. Attention is all you need. *Advances in Neural Information Processing Systems*, 2017.
- Wei, X., Yadav, A., Pascanu, R., and Gulcehre, C. Rat: Bridging rnn efficiency and attention accuracy via chunk-based sequence modeling. *arXiv preprint arXiv:2507.04416*, 2025.
- Xiao, C., Zhang, P., Han, X., Xiao, G., Lin, Y., Zhang, Z., Liu, Z., and Sun, M. Inllm: Training-free long-context extrapolation for llms with an efficient context memory. *Advances in Neural Information Processing Systems*, 37: 119638–119661, 2024a.
- Xiao, G., Tian, Y., Chen, B., Han, S., and Lewis, M. Efficient streaming language models with attention sinks. *arXiv preprint arXiv:2309.17453*, 2023.
- Xiao, G., Tang, J., Zuo, J., Guo, J., Yang, S., Tang, H., Fu, Y., and Han, S. Duoattention: Efficient long-context llm inference with retrieval and streaming heads. *arXiv preprint arXiv:2410.10819*, 2024b.
- Yang, B., Venkitesh, B., Talupuru, D., Lin, H., Cairuz, D., Blunsom, P., and Locatelli, A. Rope to nope and back again: A new hybrid attention strategy. *arXiv preprint arXiv:2501.18795*, 2025.
- Yang, S., Kautz, J., and Hatamizadeh, A. Gated delta networks: Improving mamba2 with delta rule. *arXiv preprint arXiv:2412.06464*, 2024.
- Yuan, J., Gao, H., Dai, D., Luo, J., Zhao, L., Zhang, Z., Xie, Z., Wei, Y., Wang, L., Xiao, Z., et al. Native sparse attention: Hardware-aligned and natively trainable sparse attention. In *Proceedings of the 63rd Annual Meeting of the Association for Computational Linguistics (Volume 1: Long Papers)*, pp. 23078–23097, 2025.
- Zaheer, M., Guruganesh, G., Dubey, K. A., Ainslie, J., Alberti, C., Ontanon, S., Pham, P., Ravula, A., Wang, Q., Yang, L., et al. Big bird: Transformers for longer sequences. *Advances in neural information processing systems*, 33:17283–17297, 2020.
- Zhang, B. and Sennrich, R. Root mean square layer normalization. *Advances in Neural Information Processing Systems*, 32, 2019.
- Zhang, J., Xiang, C., Huang, H., Xi, H., Zhu, J., Chen, J., et al. Spargeattention: Accurate and training-free sparse attention accelerating any model inference. In *Forty-second International Conference on Machine Learning*, 2025.
- Zhang, Y., Yang, S., Zhu, R.-J., Zhang, Y., Cui, L., Wang, Y., Wang, B., Shi, F., Wang, B., Bi, W., et al. Gated slot attention for efficient linear-time sequence modeling. *Advances in Neural Information Processing Systems*, 37: 116870–116898, 2024.
- Zhang, Z., Sheng, Y., Zhou, T., Chen, T., Zheng, L., Cai, R., Song, Z., Tian, Y., Ré, C., Barrett, C., et al. H2o: Heavy-hitter oracle for efficient generative inference of large language models. *Advances in Neural Information Processing Systems*, 36:34661–34710, 2023.

A. Appendix

A.1. Implementation details

Implementation for Table 1. We largely follow the RAT implementation, using the same model architecture and training dataset but also some modifications. RAT shares linear projections for attention queries and keys across heads to match the parameter count of standard attention. In our implementation, we do not take this parameter sharing; instead, we keep dense linear projection for the recurrence and leave further lightweight considerations for future work. For the results in the third block, we simply adopt full-sequence recurrence and find that it improves performance.

RAT+ pretraining For the 1.5B-parameter model, we use a model dimension of 2048, 24 Transformer layers, and a head dimension of 128, equipped with RMSNorm (Zhang & Sennrich, 2019) and no bias terms. The context window is set to 4096. We use standard RoPE (Su et al., 2024) instead of the inter-chunk RoPE used in RAT, for easier management of positional encoding, and put it after the recurrence function. The RoPE based is set to 10,000. Model parameters are initialized from a Gaussian distribution with a standard deviation of 0.02. We adopt the LLaMA2 tokenizer in all experiments.

The optimization hyperparameters follow the rule described in Bi et al. (2024). We use a cosine-annealed learning rate schedule with a peak learning rate of 8.0×10^{-4} , decaying to 1.0×10^{-6} , and 5% warmup. The global batch size is set to 512.

For the 2.6B-parameter model trained on 100B tokens, we increase the model dimension to 2560 with 28 layers. All other hyperparameters are kept the same, except that we use a peak learning rate of 7.0×10^{-4} and a global batch size of 640. For the 200B-token training setting, the peak learning rate remains 7.0×10^{-4} with a global batch size of 768, following the same rule in Bi et al. (2024).

RAT+ adapting The adaptation process uses 1B randomly sampled tokens from the FineWeb-Edu dataset. We use the original batch size and a small learning rate, e.g., $2.0e-5$. In practice, we find that the training loss during adaptation stabilizes within a few hundred million tokens, as shown in Figure Fig. 7. To ensure sufficient adaptation, we use 1B tokens in all experiments.

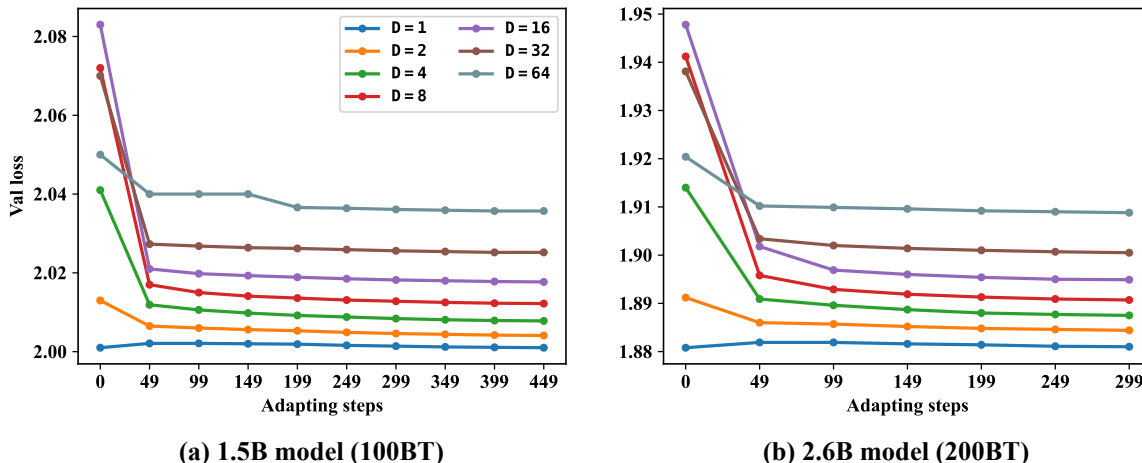


Figure 7. Validation loss curves for adapting different models with 1B tokens. It is evident that models with various dilated patterns quickly adjust and achieve stable loss values within a few hundred million tokens. We employed a simple optimization scheme with no warmup, which may explain the slight loss increase of $D = 1$ at the beginning, after which it recovers.

Evaluation Our evaluation setup largely follows the settings used in RAT, except for the NIAH tasks. We construct a dataset of approximately 7M tokens and apply a single-stage SFT before all evaluations. Compared to RAT, we sweep SFT for four epochs instead of one, to ensure that all models faithfully follow instructions.

Efficiency The decoding implementation is straightforward, requiring only a single update for the recurrence and the use of the *SDPA* kernel in PyTorch. For training and prefilling, the recurrence is implemented using the *associative scan* in

PyTorch. In the attention computation, we first use *flex attention* to handle the dilated connections by applying a dilation-level mask and returning the softmax denominator. We then compute the local and initial connections. The online softmax technique (Milakov & Gimelshein, 2018) is used to gather the results from the two parts. We expect that the efficiency of RAT+ can be further improved with dedicated CUDA kernel-level optimizations.

B. Supporting materials for Method

In this part, we include detailed evaluation results on commonsense reasoning tasks for Table 1 in Table 9, visualizations of the different distributions at the initial recurrence steps in Fig. 8, ablation studies for the proposed method in Table 10, and perplexity results on PG19 in Table 11.

Table 9. Detailed results of train-from-scratch models. Note that the dilated-only models fail in pretraining.

Model	ARC-C PPL	ARC-E acc_n	Hella. acc	LMB. acc_n	PIQA acc	Wino. acc	Avg. acc	-
Dilated ($D^\dagger = 8$)	-	-	-	-	-	-	-	-
RAT (L = 8, D = 8)	39.08	71.13	57.82	47.47	73.23	56.51	57.54	-
Dilated ($D^\dagger = 16$)	-	-	-	-	-	-	-	-
RAT (L = 16, D = 16)	39.76	72.6	56.95	46.03	72.14	54.46	56.99	-
Dilated ($D^\dagger = 64, W = 64$)	40.36	70.2	57.16	46.77	72.85	57.06	57.40	-
RAT (L = 64, D = 64, W = 64)	40.7	72.94	58.25	48.77	73.12	58.64	58.74	-
attention	40.1	71.84	58.5	49.95	72.42	57.14	58.33	-
attention + recurrence	40.02	72.9	58.92	49.51	73.29	58.41	58.84	-
attention - ogate	37.71	71.25	57.44	47.84	73.29	57.7	57.54	-
attention - ogate + recurrence	39.25	71.59	58.94	49.66	72.52	57.43	58.23	-

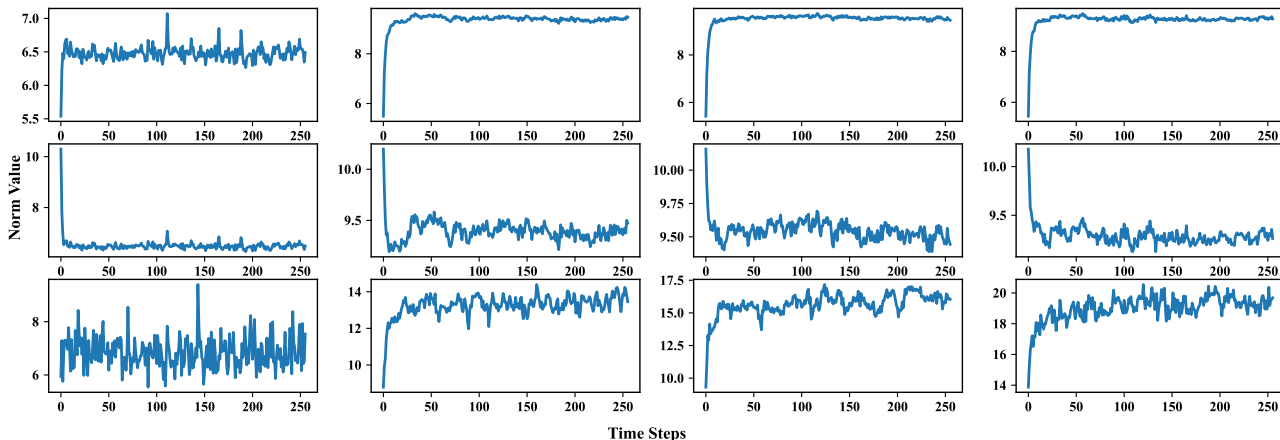


Figure 8. L2 norm values of recurrence outputs at different time steps. We observe that the outputs at early time steps differ significantly. The first row shows an initialized network using our simple recurrence at layers 0, 6, 18, and 23. The second row corresponds to the same initialized network but with a non-zero initial cell state provided to the recurrence. The third row shows the results of the pretrained network. We visualize the outputs of our simple recurrence here; a similar phenomenon has also been observed in standard recurrent networks, as reported in Cooijmans et al. (2016).

C. Additional downstream evaluation results

In this part, we provide additional downstream evaluation results on the remaining LongBench tasks in Table 12, on NIAH tasks in Table 13, Table 14 and Table 15, and evaluation results of 2.6B model in Table 16. We observe an interesting difference between dilated attention and top-k block attention on the NIAH tasks. Dilated attention appears to find NIAH-S-3 more challenging than NIAH-MK-2, NIAH-MQ, and NIAH-MV, with worse performance on NIAH-S-3. In contrast, top-k

Table 10. Ablation studies of RAT+. All configurations are adapted from the corresponding pretrained models with 1B tokens, except for the w/o adaptation case. In the RAT+ ablation block: (1). the first row sets L equal to D at inference, and thus suffers from distribution shifts at the initial recurrence steps, leading to poor performance at $D = 1$; (2). The second row performs worse than RAT+ because dense connectivity is not sufficiently learned; (3). The third row removes active recurrence learning, although dense performance is preserved, recurrence is not learned effectively, resulting in degraded performance at larger dilation sizes due to an incomplete receptive field; (4). The fourth row shows results without adaptation for our final variant. Note that even $D = 64$ still requires adaptation, since four initial tokens are additionally added at inference.

Model	Train	Inference (D value)						
		1	2	4	8	16	32	64
RAT+								
L = 64	D = 1, D = 64	7.4	7.42	7.45	7.48	7.52	7.58	7.67
L = T, L* = 64	D = 1, D = 64	7.4	7.42	7.45	7.48	7.52	7.58	7.66
RAT+ ablations								
L = 64 (L = D adapt)	D = 1, D = 64	8.39	8.14	7.84	7.68	7.6	7.6	7.66
L = 64	$0.5\mathcal{L}_{D=64} + 0.5\mathcal{L}_{D=1}$	7.52	7.56	7.58	7.62	7.66	7.73	7.82
L = T	D = 1	7.39	7.77	8.18	8.66	9.16	9.60	9.96
L = T, L* = 64 (w/o adapt)	D = 1, D = 64	7.4	7.49	7.69	7.94	8.03	7.93	7.77
attention baselines								
-	$D^\dagger = 1$	7.44	17.12	40.71	65.05	87.88	109.8	129.3
-	$D^\dagger = 1, W = 64$	7.41	16.73	40.24	64.28	87.21	109.3	129.1
-	$D^\dagger = 1, D^\dagger = 64$	7.82	16.22	34.74	52.96	70.94	90.1	109.9
RAT (L = 16)	D = 16	8.41	8.08	7.79	7.64	7.61	7.74	7.93

Table 11. PPL performance of a 200M RAT+ model on the PG19 book dataset with a context length of 8192. The first row shows strong performance across dilation settings. The second and third rows report additional design-choice ablations. As can be seen, removing recurrence over the attention keys leads to a slight increase in perplexity. We think this might be because the gated representations on the attention values can still be propagated across layers. In contrast, applying recurrence to the input of the qkv projections results in clear worse performance, with $D = 4$ even higher than the $D = 128$ setting of the standard RAT+ variant.

Model	Inference (D value)							
	1	2	4	8	16	32	64	128
RAT+ (L = T, L* = 128)	10.71	10.87	10.97	11.05	11.15	11.20	11.28	11.39
RAT+ (w/o recurrence on key)	11.68	11.03	11.23	11.32	11.36	11.40	11.44	11.47
Recurrence on input for qkv projections	11.01	11.26	11.44	11.59	11.72	11.83	11.95	12.09

block attention treats NIAH-S-3 as an easier task relative to these three. We think this reflects the interaction between task characteristics and sparsification patterns. NIAH-S-3 and NIAH-MK-3 involve retrieving 32-digit UUID strings, where dilated attention with large dilation sizes may fail to capture the exact sequence; even a single incorrect digit leads to a complete loss of score. On the other hand, MQ, MV, and MK tasks involve multiple keys, queries, and values, which place a heavier burden on top-k block attention to identify the critical blocks, especially under less favorable configurations of D and K.

Table 12. Supplementary results on additional LongBench tasks. We omit these results from the main text as they are less representative. All models perform poorly on MusiQue and exhibit very similar performance on LCC. For the remaining summarization tasks, we observe that pretrained-only models tend to repeat prompts or outputs, which makes the quantitative results less reliable. But it can be seen that our dilated attention maintains performance close to the dense baseline with the gap generally increases as the dilation size becomes larger.

RAT+ ($L^* = 64$)	Musique	GovReport	QMSUM	MultiNews	LCC
T = 4096					
D = 1	7.2	15.34	17.56	18.25	19
D = 2	7.85	16.13	17.47	16.51	19.1
D = 4	7.59	15.45	17.22	18	19.69
D = 8	7.81	13.98	16.6	15.37	19.1
D = 16	7.61	15.1	16.36	16.08	18.37
D = 32	6.92	12.45	15.6	14.75	17.96
D = 64	6.85	12.47	15.17	16.07	18.26
D = 128	6.9	11.82	15.06	15.48	18.8
NTK extended					
T = 16384					
D = 1	7.62	21.87	17.86	18.45	18.81
D = 4	7.44	21.72	17.97	19.56	18.55

Table 13. **Retrieval ability:** Accuracy performance with exact match scoring on the Needle-in-Haystack tasks with different configurations from the RULER benchmark (Hsieh et al., 2024). We use T = 4096 and bold less favorable results. We found they mainly occur when the text query/key/values are the UUID, and may wrongly copied part of the answers. Also, in NIAH-MK-2, bigger dilation size also performs worse.

SFT models	NIAH-S-1	NIAH-S-1	NIAH-S-3	NIAH-MK-1	NIAH-MK-2	NIAH-MK-3	NIAH-MQ	NIAH-MV
D = 1	100	100	100	100	100	99.6	99.85	100
D = 2	100	100	99.2	100	99.2	96	99.8	99.8
D = 4	100	100	97.8	99.8	97.4	88.8	99.75	99.5
D = 8	100	100	96	99.8	96.4	73.8	99.4	99.15
D = 16	100	100	89.2	99.6	95.2	54.6	99.3	98.15
D = 32	100	100	78.8	99.2	78	40.4	97.35	96.35
D = 64	100	100	76	98.4	46.8	30	97.35	93.9

D. Additional efficiency results

In this part, we provide detailed and more efficiency results in Table 17, Table 18, Table 20, and Table 20. We also mark out some speed-ups in the tables.

Table 14. Retrieval ability of the top-k block attention for different models. On the following three pretrained plus SFT models, we apply Quest (Tang et al., 2024) style top-k block attention, where the critical block is determined by the Min/Max statistics of attention keys within each block.

Quest top-k	NIAH-S-1	NIAH-S-1	NIAH-S-3	NIAH-MK-1	NIAH-MK-2	NIAH-MK-3	NIAH-MQ	NIAH-MV
attention								
$D^\dagger = 1$, All	100	100	99.8	100	100	99.6	100	99.9
$D^\dagger = 16$, $K = 16$	100	99.8	99.4	99.6	71.2	5.4	93.95	94.25
$D^\dagger = 16$, $K = 64$	100	100	100	100	99.6	85.2	99.9	99.6
$D^\dagger = 64$, $K = 8$	100	100	85.8	98.4	20.6	0.2	87.55	88.55
$D^\dagger = 64$, $K = 16$	100	100	99	99.8	63.2	15.2	97.45	96.85
RAT+								
$D = 1$, All	100	100	100	100	100	99.6	99.85	100
$D = 16$, $K = 16$	100	100	100	100	97.6	94.8	99.85	99.9
$D = 16$, $K = 64$	100	100	100	100	100	99.2	100	99.95
$D = 64$, $K = 8$	100	100	99.8	100	57.4	11	98.75	99.7
$D = 64$, $K = 16$	100	100	100	100	93.8	51.6	99.85	99.95
RAT+ (no ARL in SFT)								
$D = 1$, All	100	100	100	100	99.4	98.8	99.8	99.85
$D = 16$, $K = 16$	100	100	100	100	84.2	27.4	96.95	99.4
$D = 16$, $K = 64$	100	100	100	100	99.2	97.6	99.7	99.85
$D = 64$, $K = 8$	100	100	100	99.8	32	5.4	90.25	98.55
$D = 64$, $K = 16$	100	100	100	100	76.8	28	98.05	99.6

Table 15. Retrieval ability of the top-k block attention for different models. On the following three pretrained plus SFT models, we apply MoBA (Lu et al., 2025) style top-k block attention, where the critical block is determined by the mean pooling of attention keys within each block. We found that this style performs worse than the Quest in the training-free manner, but RAT+ still outperforms the baseline a lot.

MoBA top-k	NIAH-S-1	NIAH-S-1	NIAH-S-3	NIAH-MK-1	NIAH-MK-2	NIAH-MK-3	NIAH-MQ	NIAH-MV
attention								
$D^\dagger = 1$, All	100	100	99.8	100	100	99.6	100	99.9
$D^\dagger = 16$, $K = 16$	100	91	56	84	65.2	6.2	48.1	55.9
$D^\dagger = 16$, $K = 64$	100	99.8	96.2	99.6	97.8	77	95.35	96.45
$D^\dagger = 64$, $K = 8$	90.2	66.8	20	54.2	29.8	5.8	30.1	34.55
$D^\dagger = 64$, $K = 16$	99.2	95.8	79	91.8	66.2	22.6	70.7	76.35
RAT+								
$D = 1$, All	100	100	100	100	100	99.6	99.85	100
$D = 16$, $K = 16$	100	100	97.8	100	96.4	86.8	99.15	99.7
$D = 16$, $K = 64$	100	100	99.8	100	99.8	99.2	100	99.95
$D = 64$, $K = 8$	98.4	99.6	79.6	95.4	39.4	10.8	81.55	88.1
$D = 64$, $K = 16$	99.8	100	96.8	99.8	80.2	40.2	96.55	98.2

Table 16. Performance of 2.6B RAT+ on common-sense reasoning tasks ($T \leq 300$) pretrained on 100B and 200B tokens, respectively. We use $L^* = 64$ and enable the $D = 128$ setting via length generalization of the recurrence.

2.6B Model	ARC-C	ARC-E	Hella.	LMB.	PIQA	Wino.	Avg.
	acc_n	acc	acc_n	acc	acc	acc	-
RAT+ (100BT)							
D = 1	44.2	75.42	62.85	52.14	74.37	60.54	61.59
D = 2	44.03	75.34	62.67	51.52	74.32	59.43	61.22
D = 4	44.71	75.84	62.65	50.79	73.99	59.51	61.25
D = 8	43.52	75.88	62.61	50.28	74.27	58.48	60.84
D = 16	44.03	75.63	62.34	49.95	74.1	58.33	60.73
D = 32	43.34	75.25	62.01	48.01	73.99	57.38	60.00
D = 64	43.77	75.51	61.35	45.62	74.27	56.59	59.52
D = 128	43.34	75.67	61.08	43.53	74.21	57.38	59.20
RAT+ (200BT)							
D = 1	44.62	76.35	65.28	54.18	75.24	60.54	62.70
D = 2	44.88	76.26	65.15	53.48	75.41	60.3	62.58
D = 4	44.88	76.14	65.17	53.13	75.3	60.22	62.47
D = 8	43.94	75.84	64.71	52.86	75.46	58.8	61.94
D = 16	44.11	75.93	64.36	52.05	75.68	58.64	61.80
D = 32	43.86	75.8	63.81	50.9	75.73	58.17	61.38
D = 64	44.11	75.97	63.48	48.52	75.57	58.87	61.09
D = 128	43.69	76.26	62.99	46.5	75.68	58.17	60.55

Table 17. Temporal-mixing operator and block (linear projections included) prefilling time across different sequences lengths for hidden dimension 2048. The latency (ms) is tested on 262K sequences of tokens. $D^\dagger = 1$ means the attention operator or block without the recurrence.

Latency (H=2048)	4K	8K	16K	32K	65K	131K	262K
Temporal-mixing operator							
$D^\dagger = 1$	16.3	28.5	51.8	101.1	197.9	422.3	897.8
$D = 1$	32.0	43.9	67.8	118.2	218.4	445.3	942.4
$D = 2$	30.9	37.9	51.9	83.3	144.2	280.1	587.5
$D = 4$	26.9	30.6	37.7	54.2	87.6	165.4	330.7
$D = 8$	24.3	25.9	29.1	37.7	54.4	98.7	190.9
$D = 16$	23.3	24.3	26.1	31.4	42.8	74.5	143.6
$D = 32$	23.1	23.5	24.3	28.3	36.3	62.0	119.4
$D = 64$	22.8	23.3	23.7	26.8	33.6	56.2	107.9
$D = 8, W = 512$	27.2	29.1	32.0	40.2	58.0	101.8	199.4
$D = 16, W = 256$	25.2	26.1	27.9	33.3	44.3	76.5	148.6
$D^\dagger = 1 / D = 16$	$0.7\times$	$1.2\times$	$2.0\times$	$3.2\times$	$4.6\times$	$5.7\times$	$6.3\times$
$D = 1 / D = 16$	$1.4\times$	$1.8\times$	$2.6\times$	$3.8\times$	$5.1\times$	$6.0\times$	$6.6\times$
Temporal-mixing block							
$D^\dagger = 1$	40.3	54.5	78.4	125.9	227.3	441.9	936.6
$D = 1$	59.9	75.5	98.0	149.5	248.5	464.8	972.7
$D = 2$	59.4	67.2	83.1	115.7	182.3	316.5	614.2
$D = 4$	54.6	57.5	67.9	85.5	120.3	198.7	359.7
$D = 8$	51.9	53.4	57.0	65.4	82.5	121.0	221.2
$D = 16$	48.8	51.6	53.8	59.8	72.5	102.5	177.0
$D = 32$	49.6	50.7	51.4	55.8	61.6	89.2	146.6
$D = 64$	50.3	50.4	50.6	51.0	61.6	79.5	133.7
$D = 8, W = 512$	53.5	56.7	60.8	66.3	88.2	126.0	223.7
$D = 16, W = 256$	53.0	53.5	55.3	60.7	71.7	103.2	179.5
$D^\dagger = 1 / D = 16$	$0.8\times$	$1.1\times$	$1.5\times$	$2.1\times$	$3.1\times$	$4.3\times$	$5.3\times$
$D = 1 / D = 16$	$1.2\times$	$1.5\times$	$1.8\times$	$2.5\times$	$3.4\times$	$4.5\times$	$5.5\times$

Table 18. Decoding latency of temporal-mixing operator and blocks for hidden dimension 2048. The latency (ms) is tested on generating batches of tokens with $B = 128$, $B = 256$, $B = 512$ at specified positions.

Latency (H=2048)	4K	8K	16K	32K	65K	131K	262K
Temporal-mixing operator							
$B = 128$							
$D^\dagger = 1$	1.19	2.33	4.62	9.18	18.34	OOM	OOM
$D = 1$	1.24	2.38	4.67	9.24	18.38	OOM	OOM
$D = 2$ (vs. $D^\dagger = 1$)	0.69 (1.7 \times)	1.26 (1.8 \times)	2.37 (1.9 \times)	4.66 (2.1 \times)	9.22 (2.0 \times)	18.35	OOM
$D = 4$	0.49	0.69	1.26	2.37	4.66	9.23	18.35
$D = 8$	0.47	0.58	0.69	1.26	2.37	4.66	9.22
$D = 16$	0.45	0.43	0.47	0.69	1.26	2.38	4.66
$D = 32$	0.39	0.41	0.45	0.59	0.69	1.26	2.37
$D = 64$	0.36	0.48	0.44	0.45	0.48	0.69	1.26
$D = 8, W = 512$	0.55	0.62	0.82	1.41	2.59	4.91	9.63
$D = 16, W = 256$	0.48	0.5	0.54	0.76	1.35	2.51	4.85
$B = 256$							
$D^\dagger = 1$	2.32	4.58	9.08	18.07	OOM	OOM	OOM
$D = 1$	2.38	4.64	9.14	18.14	OOM	OOM	OOM
$D = 2$ (vs. $D^\dagger = 1$)	1.27 (1.8 \times)	2.41 (1.9 \times)	4.63 (2.0 \times)	9.13	18.13	OOM	OOM
$D = 4$	0.7	1.27	2.41	4.63	9.13	18.13	OOM
$D = 8$	0.49	0.7	1.27	2.41	4.63	9.13	18.13
$D = 16$ (vs. $D^\dagger = 1$)	0.44 (5.3 \times)	0.55 (8.3 \times)	0.7 (13.0 \times)	1.27 (14.2 \times)	2.41	4.63	9.14
$D = 32$	0.42	0.55	0.49	0.7	1.27	2.41	4.64
$D = 64$	0.38	0.47	0.5	0.49	0.7	1.27	2.41
$D = 8, W = 512$	0.68	0.99	1.54	2.72	5.03	9.66	18.92
$D = 16, W = 256$	0.63	0.56	0.84	1.42	2.58	4.9	9.53
$B = 512$							
$D^\dagger = 1$	4.59	9.09	18.08	OOM	OOM	OOM	OOM
$D = 1$	4.65	9.15	18.14	OOM	OOM	OOM	OOM
$D = 2$	2.43	4.71	9.15	18.15	OOM	OOM	OOM
$D = 4$	1.29	2.43	4.71	9.16	18.14	OOM	OOM
$D = 8$	0.72	1.29	2.43	4.72	9.15	18.14	OOM
$D = 16$ (vs. $D^\dagger = 1$)	0.45 (10.2 \times)	0.72 (12.6 \times)	1.29 (14.0 \times)	2.43	4.71	9.16	18.15
$D = 32$	0.49	0.45	0.72	1.29	2.43	4.71	9.15
$D = 64$ (vs. $D = 16$)	0.46 (1.0 \times)	0.47 (1.5 \times)	0.51 (2.5 \times)	0.72 (3.4 \times)	1.29 (3.7 \times)	2.43 (3.8 \times)	4.71 (3.9 \times)
$D = 8, W = 512$	1.25	1.86	2.96	5.3	9.95	19.23	OOM
$D = 16, W = 256$	0.71	0.99	1.57	2.73	5.05	9.68	18.91
Temporal-mixing block							
$B = 512$							
$D^\dagger = 1$	4.72	9.21	18.22	OOM	OOM	OOM	OOM
$D = 1$	4.8	9.29	18.29	OOM	OOM	OOM	OOM
$D = 2$ (vs. $D^\dagger = 1$)	2.58 (1.8 \times)	4.86 (1.9 \times)	9.31 (2.0 \times)	18.3	OOM	OOM	OOM
$D = 4$ (vs. $D^\dagger = 1$)	1.44 (3.3 \times)	2.58 (3.6 \times)	4.86 (3.7 \times)	9.31	18.3	OOM	OOM
$D = 8$	1	1.45	2.58	4.87	9.31	18.29	OOM
$D = 16$ (vs. $D^\dagger = 1$)	0.88 (5.4 \times)	1.13 (8.2 \times)	1.45 (12.6 \times)	2.59	4.87	9.32	18.31
$D = 32$	0.83	0.93	1.06	1.45	2.59	4.87	9.32
$D = 64$	0.76	0.77	0.92	1.01	1.45	2.59	4.87
$D = 8, W = 512$	1.4	2.01	3.11	5.46	10.1	19.38	OOM
$D = 16, W = 256$	0.98	1.18	1.72	2.88	5.2	9.84	19.08

Table 19. Temporal-mixing operator and block (linear projections included) prefilling time across different sequences lengths for hidden dimension 4096. The latency (ms) is tested on 262K tokens. We observe even better speed-up on both operator and block levels compared to H=2048.

Latency (H=4096)	4K	8K	16K	32K	65K	131K	262K
Temporal-mixing operator							
$D^\dagger = 1$	33.23	56.90	106.03	203.94	397.90	839.06	1789.60
$D = 1$	64.36	88.78	138.34	237.04	429.17	875.68	1839.85
$D = 2$	61.77	76.53	104.56	165.74	281.48	530.33	1100.72
$D = 4$	53.81	61.16	75.78	105.75	168.60	296.81	583.40
$D = 8$	48.67	52.05	58.28	72.58	102.40	165.94	303.43
$D = 16$	46.89	48.92	52.41	59.84	77.55	117.82	211.29
$D = 32$	46.50	47.40	49.12	53.01	64.75	92.56	161.59
$D = 64$	45.81	46.99	47.76	50.02	58.52	80.46	136.50
$D = 8, W = 512$	54.21	57.21	64.32	77.57	108.21	171.87	313.64
$D = 16, W = 256$	50.32	52.03	55.85	62.88	82.04	119.74	214.41
$D = 1 / D = 16$	1.37 \times	1.81 \times	2.64 \times	3.96 \times	5.53 \times	7.43 \times	8.71 \times
$D^\dagger = 1 / D = 16$	0.71 \times	1.16 \times	2.02 \times	3.41 \times	5.13 \times	7.12 \times	8.47 \times
Temporal-mixing block							
$D^\dagger = 1$	116.53	141.30	187.46	293.98	479.93	913.62	1877.32
$D = 1$	161.27	185.54	234.56	333.38	535.64	981.81	1960.33
$D = 2$	159.13	179.87	200.92	273.59	379.28	635.22	1204.32
$D = 4$	152.13	159.08	177.93	212.50	272.70	408.52	694.38
$D = 8$	146.65	150.38	157.87	169.13	202.16	265.14	417.62
$D = 16$	146.54	146.11	151.00	158.90	179.45	219.13	313.70
$D = 32$	144.17	145.05	143.80	151.24	164.32	190.89	261.45
$D = 64$	142.80	144.58	145.22	145.94	159.37	178.21	236.68
$D = 8, W = 512$	151.38	160.30	164.59	175.73	211.21	272.00	419.63
$D = 16, W = 256$	147.94	148.05	152.04	161.56	181.04	219.94	316.19
$D = 1 / D = 16$	1.10 \times	1.27 \times	1.55 \times	2.10 \times	2.98 \times	4.48 \times	6.25 \times
$D^\dagger = 1 / D = 16$	0.80 \times	0.97 \times	1.24 \times	1.85 \times	2.67 \times	4.17 \times	5.98 \times

Table 20. Decoding latency of temporal-mixing operator and blocks for hidden dimension 4096. The latency (ms) is tested on generating batches of tokens with $B = 128$, $B = 256$, $B = 512$ at specified positions.

Latency (H=4096)	4K	8K	16K	32K	65K	131K	262K
Temporal-mixing operator							
$B = 128$							
$D^\dagger = 1$	2.32	4.58	9.08	18.09	OOM	OOM	OOM
$D = 1$	2.38	4.64	9.14	18.14	OOM	OOM	OOM
$D = 2$ (vs. $D^\dagger = 1$)	1.27 (1.8 \times)	2.42 (1.9 \times)	4.64 (2.0 \times)	9.14 (2.0 \times)	18.17	OOM	OOM
$D = 4$	0.70	1.27	2.41	4.64	9.13	18.15	OOM
$D = 8$	0.49	0.70	1.28	2.42	4.64	9.14	18.15
$D = 16$	0.41	0.48	0.71	1.28	2.42	4.64	9.15
$D = 32$	0.54	0.59	0.53	0.71	1.28	2.42	4.64
$D = 64$	0.43	0.55	0.46	0.58	0.70	1.27	2.41
$D = 8, W = 512$	0.68	0.98	1.54	2.72	5.04	9.67	18.97
$D = 16, W = 256$	0.61	0.56	0.84	1.42	2.58	4.91	9.53
$B = 256$							
$D^\dagger = 1$	4.59	9.09	18.09	OOM	OOM	OOM	OOM
$D = 1$	4.65	9.15	18.15	OOM	OOM	OOM	OOM
$D = 2$	2.43	4.72	9.15	18.15	OOM	OOM	OOM
$D = 4$	1.29	2.43	4.71	9.15	18.15	OOM	OOM
$D = 8$	0.73	1.30	2.44	4.72	9.17	18.16	OOM
$D = 16$ (vs. $D^\dagger = 16$)	0.45 (10.2 \times)	0.73 (12.5 \times)	1.30 (14.0 \times)	2.44	4.72	9.16	18.15
$D = 32$	0.48	0.50	0.73	1.30	2.44	4.72	9.16
$D = 64$	0.45	0.55	0.48	0.72	1.29	2.44	4.71
$D = 8, W = 512$	1.25	1.88	2.96	5.30	9.95	19.23	OOM
$D = 16, W = 256$	0.71	0.99	1.57	2.73	5.06	9.69	18.92
$B = 512$							
$D^\dagger = 1$	9.11	18.10	OOM	OOM	OOM	OOM	OOM
$D = 1$	9.21	18.21	OOM	OOM	OOM	OOM	OOM
$D = 2$	4.79	9.36	18.22	OOM	OOM	OOM	OOM
$D = 4$	2.50	4.79	9.35	18.22	OOM	OOM	OOM
$D = 8$	1.37	2.52	4.80	9.37	18.22	OOM	OOM
$D = 16$	0.81	1.37	2.51	4.80	9.36	18.22	OOM
$D = 32$	0.60	0.81	1.37	2.51	4.80	9.37	18.23
$D = 64$	0.54	0.60	0.81	1.37	2.51	4.79	9.35
$D = 8, W = 512$	2.41	3.69	5.84	10.53	19.78	OOM	OOM
$D = 16, W = 256$	1.35	1.90	3.06	5.38	10.02	19.29	OOM
Temporal-mixing block							
$B = 512$							
$D^\dagger = 1$	9.46	18.46	OOM	OOM	OOM	OOM	OOM
$D = 1$	9.62	18.63	OOM	OOM	OOM	OOM	OOM
$D = 2$ (vs. $D^\dagger = 1$)	5.19 (1.8 \times)	9.78 (1.9 \times)	18.64	OOM	OOM	OOM	OOM
$D = 4$	2.91	5.21	9.77	18.64	OOM	OOM	OOM
$D = 8$	1.77	2.91	5.20	9.76	18.63	OOM	OOM
$D = 16$	1.21	1.78	2.91	5.20	9.77	18.63	OOM
$D = 32$	1.01	1.21	1.77	2.92	5.20	9.76	18.63
$D = 64$	0.96	1.03	1.22	1.78	2.92	5.20	9.78
$D = 8, W = 512$	2.81	4.10	6.24	10.91	20.17	OOM	OOM
$D = 16, W = 256$	1.76	2.31	3.48	5.79	10.43	19.70	OOM